ACS APPLIED MATERIALS & INTERFACES

Research Article

www.acsami.org

Blood Compatibility of Iron-Doped Nanosize Hydroxyapatite and Its Drug Release

V. Sarath Chandra,[†] Ganga Baskar,[‡] R. V. Suganthi,[†] K. Elayaraja,[†] M. I. Ahymah Joshy,[†] W. Sofi Beaula,[‡] R. Mythili,[§] Ganesh Venkatraman,*[,‡] and S. Narayana Kalkura*[,†]

[†]Crystal Growth Centre, Anna University, Chennai 600 025, India

[‡]Department of Human Genetics, Sri Ramachandra University, Porur, Chennai 600 116, India

[§]Physical Metallurgy Division, Metallurgy and Materials Group, IGCAR, Kalpakkam, Chennai 603 102, India

ABSTRACT: Nanosize hydroxyapatite (nHAp) doped with varying levels of Fe^{3+} (Fe-nHAp of average size 75 nm) was synthesized by hydrothermal and microwave techniques. The samples were characterized for physiochemical properties by X-ray diffraction (XRD), Fourier transform infrared spectroscopy (FT-IR), inductively coupled plasma optical emission spectrometer (ICP-OES), transmission electron microscopy (TEM), vibrating sample magnetometer (VSM), mechanical and dielectric properties. The biological properties like hemocompatibility, antibacterial efficacy, in vitro bioactivity and the cell proliferation of the samples were determined. XRD pattern of the samples were of single phase hydroxyapatite. As the content of Fe^{3+} increased, the crystallite size as well as crystallinity decreased along with a morphological change from spherulites to rods. The dielectric constants and Vickers hardness were enhanced on Fe^{3+} doping. The VSM studies revealed that the saturation magnetization (M_s) and retentivity (M_r) were found to increase for Fe-nHAp. nHAp impregnated with an antibiotic as a new system for drug delivery in the treatment of chronic osteomyelitis was also attempted. The in vitro drug release with an antibiotic amoxicillin and anticancer drug 5-fluorouracil showed sustained release for the lowest concentration of Fe^{3+}, while with an increase in the content; there was a rapid release of the drug. The hemolytic assay of Fe^{3+} doped samples revealed high blood compatibility (<5% hemolysis). The antibacterial activities of the antibiotic impregnated materials were tested against a culture of *E. coli, S. epidermidis* and *S. aureus* by agar diffusion test. The in vitro bioactivity test using simulated body fluid (SBF) showed better bone bonding ability by the formation of an apatite layer on the doped samples. The growth of the apatite layer on the samples surface has been confirmed by EDS analysis. The proliferative potential of MG63 cells by MTT assay confirmed the noncytotoxicity of the samples.

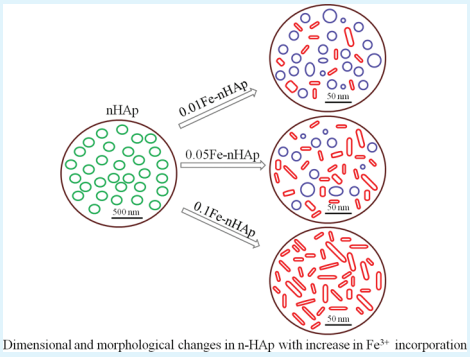

Dimensional and morphological changes in n-HAp with increase in Fe^{3+} incorporation

KEYWORDS: *nanosize hydroxyapatite, biocompatibility, drug release, hemolysis, osteomyelitis*

1. INTRODUCTION

Hydroxyapatite (HAp, $Ca_{10}(PO_4)_6(OH)_2$) is the main inorganic component of hard tissues like bone and dental reparation and also for the applications in drug delivery systems.[1,2] HAp exhibits excellent properties, like high osteoconductivity and osteoinduction when implanted in the human body.[3] HAp is an elective material because it is biocompatible, nontoxic in nature, and has been developed as a drug carrier for treating bone infections at specific sites. HAp-loaded with therapeutic concentrations of antibiotics like cephalexin or norfloxacin, amoxicillin, ciprofloxacin, gentamycin has been tested for the treatment of osteomyelitis and hence HAp can be a useful drug delivery system (DDS).[4−7] Recently, HAp has been shown to accelerate the healing of bone fractures upon electrical stimulation.[8] This response to electrical stimulation has been attributed to the porosity and microstructure of HAp. Such approaches have been documented in the treatment of osteoarthritis and osteonecrosis.[9,10] The main drawback of this material is the lack of mechanical properties which lead to implant failures. To improve these mechanical properties, several groups, including ours, have investigated numerous approaches.[11] Among these methods, formation of HAp composites by doping with different ions and through sintering has been shown to enhance the mechanical properties of HAp.[12,13] Jadalannagari et al reported the synthesis of hydroxyapatite nanorods modified by sol−gel at low temperature having the average diameter of 25 nm.[14] Recent developments on nanophase HAp bioceramics and its applications in the biomedical field have been reviewed by Zhou and Lee.[15] It was reported that nHAp, increased the cell viability and cell proliferation.[16,17] Huang et al found that the incorporation of Ti into nHAp decreased the grain size with increase in Ti. Further, Ti-HAp demonstrated better in vitro bioactivity and HOB cells proliferation.[18]

Received: July 13, 2011
Accepted: February 8, 2012
Published: February 8, 2012

HAp doped with divalent (i.e., Mg^{2+}, Zn^{2+}) and trivalent (i.e., La^{3+}, Y^{3+}, In^{3+}, Bi^{3+}) cations showed higher rates of osteoblast adhesion when compared to the undoped HAp.[19] HAp specimens with calcium ions (Ca^{2+}) substituted by different metal ions, such as Ni^{2+}, Co^{2+}, Al^{3+}, and La^{3+} were reported to have different surface configurations, morphologies, and crystal architectures depending on the amounts of metal ions present.[20] Recently, our group has reported that Sr^{2+}-doped HAp exhibit prolonged drug release profiles, effective against microbes involved in bone infections.[21] We have also reported that La^{3+}-doped nHAp have enhanced mechanical properties and behave as a sustained drug release system.[11] The biomagnetic nanoparticles of HAp incorporating some magnetic ions, exhibit strong ferromagnetic properties, play an important role in medicine for example, iron (Fe), cobalt (Co), nickel (Ni), etc., by substituting Ca^{2+} in HAp could be useful for biological applications such as magnetic resonance imaging (MRI), cell separation, drug delivery and heat mediator for the hyperthermia treatment of cancers.[22] It has been shown that HAp containing 40 wt % iron oxide-HAp is not detrimental to the osteoblast cell activity and has high X-ray opacity compared to the lower percentage of iron oxide HAp.[23] In the human body, high concentrations of iron is present in soft organs where it is readily exchanged, whereas it is present in low concentration in hard tissues without disturbing the apatite structure. It has been shown that as Fe (II) concentration increases in the Fe-HAp then the crystallinity is lowered.[24] Magnetic-Hydroxyapatite (Fe-HAp) nanoparticles when tested on mouse embryonic fibroblast cell line (3T3) elicited no cytotoxicity.[25] Iron is a micronutrient essential for various biological processes and is an important component of several metalloproteins. Iron represents approximately 35 and 45 mg/kg of body weight in adult women and men. In the intestinal lumen, iron exists in the forms of ferrous and ferric salts. However, most dietary inorganic iron is in the form of ferric salts.[26]

There are various techniques reported to date for the synthesis of ion incorporated nHAp, which includes, wet chemical,[27] gel,[28] sol–gel,[29] hydrothermal,[30] microwave[31] methods. Among this hydrothermal method has a unique property of generating materials of high crystallinity with a better control over its particle size and shape.[32] Similarly, HAp synthesis has also been attempted using the microwave method, which is a convenient, rapid and efficient method for the preparation of nanostructured inorganic materials.[33,34] Microwave and hydrothermal techniques were applied together by Han et al to synthesize needles and spherulites of nHAp.[35]

In this paper, we report the synthesis of nHAp and Fe^{3+}-doped nHAp (Fe-nHAp) by hydrothermal and microwave treatment. The synthesized samples were characterized by XRD, FT-IR, ICP-OES, TEM, VSM, mechanical and dielectric analysis. The in vitro blood compatibility, drug release using an antibiotic and an anticancer drug, bioactivity test through SBF and the antibacterial efficacy against *E. coli*, *S. epidermidis*, and *S. aureus* by agar diffusion test was studied.

2. EXPERIMENTAL PROCEDURE

a. Preparation of Undoped and Fe^{3+}-Doped nHAp. The undoped and Fe^{3+} doped nHAp powder was synthesized using calcium nitrate tetrahydrate ($Ca(NO_3)_2{\cdot}4H_2O$, Merck), diammonium hydrogen phosphate ($(NH_4)_2HPO_4$, Merck), ferric chloride ($FeCl_3$, Qualigens), and ammonia solution (analar grade).

1.0 M of $Ca(NO_3)_2{\cdot}4H_2O$ solution was prepared along with the various concentration of $FeCl_3$ (0.01 M, 0.05 and 0.1 M). This solution was added dropwise into 0.6 M of $(NH_4)_2HPO_4$ solution with vigorous stirring for 2 h at room temperature. During the reaction, the pH of the solution was maintained at 10 using ammonia solution. After mixing, the precipitated solution was subjected to hydrothermal treatment at 150 °C for 3 h (pressure developed inside the Teflon lined chamber was 120 psi). After the hydrothermal treatment, the precipitated solution was further subjected to microwave irradiation (house-hold microwave oven, 900 W and 2.45 GHz) for about 30 min. Then the samples were washed with deionized water and dried at 70 °C in a hot air oven. The undoped sample was prepared by the same experimental procedure without $FeCl_3$. Hereafter, the samples doped with 0 M $FeCl_3$, 0.01 M $FeCl_3$, 0.05 M $FeCl_3$, and 0.1 M $FeCl_3$ were labeled as 0Fe, 0.01Fe, 0.05Fe, and 0.1Fe, respectively. The physicochemical and biological properties of the prepared samples were characterized by different techniques. The powder samples were prepared as pellets of 8 mm diameter and 1 mm thickness by applying a pressure of 2 tons using hydraulic press and used for further studies.

b. In vitro Drug Release. To investigate the drug release, we determined the maximum absorbance wavelength (λ_{max}) of amoxicillin and 5-Fluorouracil as 230 and 265 nm, respectively, using UV–vis spectrophotometer.

The in vitro release profile of amoxicillin and 5-fluorouracil were conducted in phosphate buffer saline (PBS, pH 7.4) using incubated shaker. 100 mg of 0Fe, 0.01Fe, 0.05Fe, and 0.1Fe powder samples were mixed with 50 mg of amoxicillin or 5-fluorouracil are made into pellets. These pellets were immersed into 200 mL of PBS was maintained at 37 °C with shaking speed of 100 rpm. At various time intervals, 1 mL of PBS was withdrawn and replaced with fresh medium. The concentration of the released amoxicillin or 5-fluorouracil was estimated from the calibration graph. The experiments were performed in triplicate.

c. In vitro Blood Compatibility Assay. Acid citrate dextrose (ACD) human blood was used for the hemolytic assay. ACD solution was prepared by mixing 0.544 g of anhydrous citric acid, 1.65 g of trisodium citrate dihydrate, and 1.84 g of dextrose monohydrate. ACD blood was prepared by adding 1 mL of ACD solution to 9 mL of fresh human blood. Initially, the pellets of 0Fe, 0.01Fe, 0.05Fe, and 0.1Fe were sterilized under UV for 1 h. The sterilized pellets were equilibrated with 1 mL of saline for about 24 h in sterile centrifuge tubes at 37 °C in an incubator subsequently the saline was removed and 0.25 mL of ACD blood was added and incubated for 20 min. Afterward, 2 mL of sterile saline was added to stop hemolysis and were incubated for 1 h then the pellets were spun at 750G for 5 min. Human blood with deionized water served as the positive control and sterile saline served as the negative control. The supernatants were transferred into a sterile 96 well culture plate and the absorbance in the assay was measured using THERMO ELECTRON CORPORATION spectrophotometer Multiskan Spectrum at 545 nm.[36]

Percentage of hemolysis is calculated using the formula[37]

$$\%\ \text{hemolysis} = \frac{\text{OD for the test sample} - \text{OD for the negative control}}{\text{OD for the positive control} - \text{OD for the negative control}}$$

The calculated percentages of hemolysis for all the samples were compared with ASTM standard[38]

highly hemocompatible (<5% hemolysis)

hemocompatible (within 10% hemolysis) and

non-hemocompatible(>20% hemolysis)

d. In vitro Bioactivity through SBF. The apatite growth on the 0Fe, 0.01Fe, 0.05Fe, and 0.1Fe pellet samples and its bonding ability with bone were studied by in vitro bioactivity test. One hundred milligrams of the powdered samples was weighed and pressed into pellets of about 8 mm diameter and 1 mm thickness and subsequently

the pellet was weighed (W_1). Then the pellet was immersed in 20 mL of SBF in an airtight plastic container. The SBF solution was prepared by dissolving the reagent grade chemicals of NaCl, $NaHCO_3$, KCl, $K_2HPO_4{\cdot}3H_2O$, $MgCl_2{\cdot}6H_2O$, 1 M HCl, $CaCl_2{\cdot}2H_2O$, Na_2SO_4, and $((HOCH_2)_3CNH_2)$ (TRIS) in deionized water and buffered to pH 7.4 at 37 ± 0.1 °C with HCl.[39] The solution was renewed once in every two days for a period of three weeks. After 3 weeks, the pellets were taken out from the SBF solution and allowed to air-dry at 37 ± 0.1 °C. Then the pellets were reweighed (W_2). Therefore, the percentage of weight gain of the sample was calculated by $((W_2 - W_1)/W_1)100$.[40] The surface morphology of undoped and doped samples was then observed by scanning electron microscope (SEM, LEO 440 STEREO-SCAN, Leica).

e. Agar Diffusion Test. Three hundred microliter volumes of bacterial suspensions of *S. aureus, E. coli*, and *S. epidermidis* were spread uniformly on the agar plate. 0Fe, 0.01Fe, 0.05Fe, and 0.1Fe pellets and amoxicillin-impregnated 0Fe, 0.01Fe, 0.05Fe, and 0.1Fe pellets were then placed on the agar. The plates were incubated at 37 °C for 24 h and the zone of inhibition was recorded.

f. Cell Proliferation Assay. Human osteoblast-like MG-63 cells (derived from human osteosarcoma) was obtained from NCCS-Pune and cultured in 25 cm^2 cell culture flask at 37 °C in Dulbecco's Modified Eagles Medium (DMEM) (Invitrogen, USA) supplemented with 10% fetal bovine serum (FBS) (Invitrogen, USA) and 1% penicillin and streptomycin in a 5% CO_2 incubator. When the cells attained confluency, they were detached using 0.25% Trypsin/EDTA (Invitrogen, USA) and seeded onto 48-well plates (Axygen, California) at a cell density of 5×10^3 cells per well. The seeded cells were incubated overnight to allow cell adherence at 37 °C in 5% CO_2 atmosphere and was further used for cell proliferation study on the undoped and Fe^{3+}-doped samples. The samples (in pellet form with 8 mm diameter and 1 mm thickness) were placed on the attached MG-63 cells and the percentage of viable cells was assessed by MTT assay on days 1 and 3 with three trials each and compared with controls (nontreated cells and Triton-X-100). All the samples were sterilized before starting the study. At the end of the time period, 50 μL of MTT reagent (5 μg/mL) was added to each well and incubated for 2−4 h at 37 °C. The water-insoluble formazan product was dissolved by adding 500 μL of dimethylsulfoxide (DMSO) (Sigma-Aldrich) and absorbance was measured at 570 nm in an ELISA (Thermo Scientific) reader.

g. Characterization. Powder XRD was carried out on undoped and doped nHAp samples (Fe-nHAp) using Rigaku Ultima(III), CuKα radiation (λ = 0.154 nm), two theta range of 20−65° with scan speed 2°/min and step rate 0.02 per second in order to determine the crystal structure. The Scherrer equation was used to calculate the crystallite size, $D = K\lambda/\beta\cos\theta$, where K is the shape factor (0.9), β is the broadening of the full width at half-maximum (fwhm) of the diffraction peak measured in radians, λ is the wavelength of the X-rays and θ is the Bragg's diffraction angle. The crystallinity (X_c) was determined by an empirical relation between X_c and $\beta_{(002)}$[41], i.e., $\beta_{(002)} \times \sqrt[3]{X_c} = K_A$ where, $\beta_{(002)}$ is fwhm of (002) in degrees and K_A is a constant (0.24). The lattice parameters and the volume were determined by XRDA software.[42]

FT-IR spectroscopy was adopted to identify the functional groups of undoped and doped samples using PERKIN ELMER Spectrum RX1 by KBr pellet technique. The spectra were recorded from 4000 to 400 cm^{-1} in transmission mode.

The elemental compositions of Ca, P and Fe content were determined with ICP-OES using an Optima 5300 DV (Perkin-Elmer) instrument. The doped and undoped powder sample of about 0.1 g were dissolved in 1 mL of concentrated HCl and then made up to 50 mL of triple distilled water and analyzed.

The size and shape of undoped nHAp and Fe-nHAp are viewed under TEM. The samples were dispersed in acetone followed by ultra-centrifugation for 5 min. A small drop from the supernatant was dispersed and dried on a carbon-coated copper grids for TEM analysis (Philips-CM200 analytical transmission electron microscope at an operating voltage of 200 kV).

The magnetic measurements were carried out by VSM at room temperature using Lakeshore VSM 7410 instrument in an applied magnetic field of ±2 T.

The microhardness measurement was carried out using a Reichert MD 4000E ultra microhardness tester with a pyramidal diamond indenter. The indentation dwell time was 5 s fixed with loads of different magnitudes 5 to 45 g was applied on the undoped and Fe^{3+}-doped hydroxyapatite. The microhardness was calculated for each load marking by three indentations for each sample. The average diagonal length of the indentation mark was estimated. The Vickers' hardness (H_v) was calculated using the relation.

$$H_v = 1.8544P/d^2 \text{ kg/mm}^2$$

Where P is the applied load in kg and d is the diagonal length in μm.

The dielectric constant was measured using HIOKI 3532−50 LCR HI TESTER in the frequency range between 1×10^3 and 1×10^6 Hz. The dielectric analyses were performed at room temperature on the pellets of undoped and doped samples (8 mm diameter and 1 mm thickness). The dielectric constant (ε_r) were determined by using the formula[8]

$$C_p = \varepsilon_0\varepsilon_r A/t$$

$$\varepsilon_r = \frac{C_{pt}}{\varepsilon_0 A}$$

in which C_p is the capacitance of the samples, ε_0 the dielectric constant of the free space (8.854×10^{-12} F/m), A is the area of the dielectric, and t is its thickness.

3. RESULTS AND DISCUSSION

The XRD patterns of the undoped and Fe^{3+}-doped samples synthesized by hydrothermal and microwave techniques are as shown in Figure 1a−d. The XRD patterns were in good agreement with the standard JCPDS value of HAp (09−0432). The samples revealed no secondary phases other than that of nHAp. The average crystallite size and degree of crystallinity for the doped and undoped samples were calculated for all the planes. With an increase in Fe^{3+} concentration, the peak

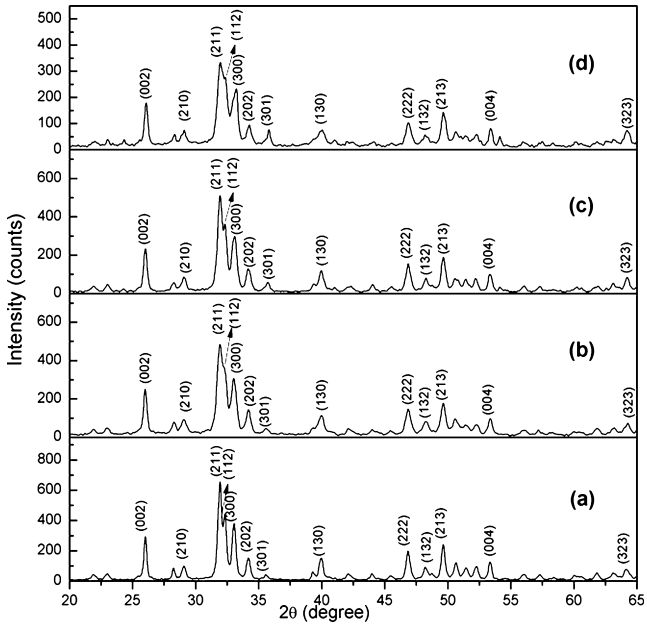

Figure 1. XRD patterns of Fe^{3+} doped and undoped HAp samples (a) 0Fe, (b) 0.01Fe, (c) 0.05Fe, and (d) 0.1Fe.

intensities were found to decrease with an increase in peak broadening, indicating a decrease in average crystallite size and crystallinity (Table 1). XRD pattern of Fe-nHAp does not show

Table 1. Crystallite Size and Crystallinity of Fe^{3+}-Doped and Undoped HAp Samples (a) 0Fe, (b) 0.01Fe, (c) 0.05Fe, and (d) 0.1Fe

samples	crystallite size (±1 nm)	crystallinity (%) (±0.01)
0Fe	33.84	98.8
0.01Fe	28.12	56.7
0.05Fe	27.46	52.8
0.1Fe	26.83	49.2

any additional peak corresponding to other phases indicating the absence of any ion exchange process which keeps the HAp structure intact.[3] The variation in lattice parameters (a and c) of the undoped and doped nHAp samples are shown in Figure 2.

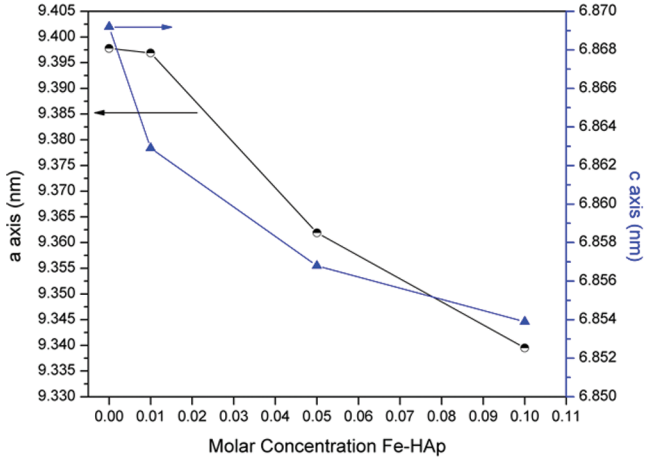

Figure 2. Lattice parameters *a* and *c*-axis of the system with increase in Fe^{3+} concentration.

The lattice parameters for both a and c slightly decreased when Ca ions are incorporated by Fe^{3+} in the nHAp. The change in lattice parameters reveals that Fe^{3+} might have entered the lattice of HAp. However, small amount of Fe^{3+} (≤90 ppm) present in the samples may not be sufficient to replace Ca^{2+} from the crystal lattice of HAp. Hence, there may be a possibility of the adsorption of Fe^{3+} ions on the surface of HAp. The ionic radius of Fe (0.645 Å) is lesser than the Ca (0.99 Å), which is in agreement (a = 9.418 Å and c = 6.884 Å) (standard values) with the observed decrease in the lattice parameters and unit-cell volume.

The FTIR spectra of the undoped and doped nHAp samples are as shown in Figure 3(a-d). The absorption bands at 633 and 3573 cm^{-1} can be ascribed to OH stretching. The peak at 1630 cm^{-1} may be attributed to the water molecules present in the HAp lattice. The peak at 1384 cm^{-1} could be assigned to the vibrational mode of carbonate ions which might have been incorporated from the atmosphere during preparation.[43] The bands at 1052 and 1094 cm^{-1} belong to the triple degenerate υ_3 asymmetric P−O stretching mode. The peak observed at 962 cm^{-1} corresponds to υ_1 mode of nondegenerate P−O symmetric stretching.[44] The band at 475 cm^{-1} is attributed to the doubly degenerate of υ_2 bending of O−P−O mode. The

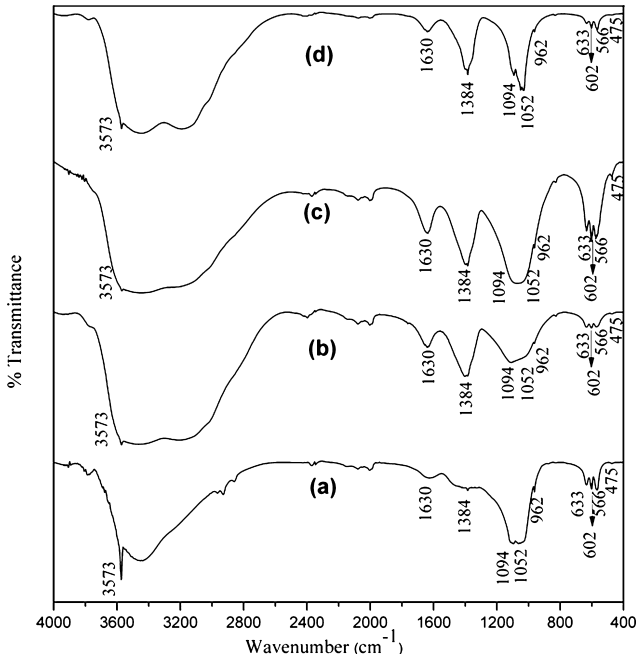

Figure 3. FT-IR spectrum for the Fe^{3+}-doped and undoped HAp samples (a) 0Fe, (b) 0.01Fe, (c) 0.05Fe, and (d) 0.1Fe.

peak at 566 and 602 cm^{-1} are assigned to the triply degenerate υ_4 bending of O−P−O mode. Similar characteristic peaks were observed for all the samples and are listed in Table 2.

Table 2. FT-IR Assignments of Functional Groups of Fe^{3+}-Doped and Undoped HAp Samples (a) 0Fe, (b) 0.01Fe, (c) 0.05Fe, and (d) 0.1Fe

assignments	IR frequency (cm^{-1})
OH stretching	3573, 1630, 633
CO_3^{2-} stretching	1384
PO_4^{3-}	962, ν_1; 475, ν_2; 1052 and1094, ν_3; 566 and 602, ν_4

Incorporation of Fe^{3+} with high Lewis acid strength results in enhanced adsorption of water and CO_2.

The elemental composition of the synthesized nHAp and Fe-nHAp determined by ICP-OES was as shown in Table 3.

Table 3. Elemental Analysis for the Fe^{3+}-Doped and Undoped HAp Samples of (a) 0Fe, (b) 0.01Fe, (c) 0.05Fe, and (d) 0.1Fe

sample code	Ca (ppm)	P (ppm)	Fe (ppm)	Ca/P	Fe/Ca %	(Ca+Fe)/P
0Fe	395.5	220.7	0	1.79		1.79
0.01Fe	352.0	179.8	7.550	1.958	2.145	2.000
0.05Fe	330.3	173.0	40.96	1.909	12.401	2.146
0.1Fe	321.0	170.2	89.99	1.886	28.034	2.414

An increase in Fe^{3+} concentration enhances the (Ca+Fe)/P ratio. As the Fe^{3+} concentration increases, there is a gradual decrease in the Ca^{2+} content in the sample. Incorporation of Fe^{3+} is found to increase with the increase in quantity of Fe^{3+} in the mother liquor (Table 4).

The TEM images of the undoped and doped nHAp samples are shown in Figure 4. The undoped sample was

dx.doi.org/10.1021/am300140q | ACS Appl. Mater. Interfaces 2012, 4, 1200−1210

Table 4. Comparison of Elemental Analysis of Fe^{3+}-Doped HAp Samples during and after Synthesis

	concentration of Fe^{3+} (ppm)	
samples	mother solution	final product
0.01 M Fe	35	7.550
0.05 M Fe	175	40.96
0.1 M Fe	349	89.99

monodispersed with spherical nHAp particles having an average size of about 200 ± 5 nm (Figure 4a), whereas 0.01Fe and 0.05Fe samples were a mixture of spheres and rods (Figure 4b, c). The 0.1Fe sample was converted fully to rodlike morphology with a drastic reduction in average particle size of about 75 nm (Figure 4d). Incorporation of about 90 ppm of Fe^{3+} into nHAp converts all the spheres into rods. The increase in Fe^{3+} incorporation seems to transform spheres into rods with a significant size reduction. The decline in size as the dopant concentration increases could probably be an advantage for the nHAp synthesized as a drug delivery vehicle.[45]

The diamagnetic property of the nHAp was revealed by VSM analysis (Figure 5a). The Fe^{3+} doped sample showed a small hysteresis loop indicating superparamagnetic behavior as shown in Figure 5b–d. As the Fe^{3+} concentration increases in HAp the maximum magnetization (M_s) and retentivity (M_r) were respectively found to be 0.2836 emu g^{-1} and 11.52 × 10^{-3} emu g^{-1} (Table 5). In the case of 0.01Fe and 0.05Fe, the distribution of Fe^{3+} might not be uniform, leading to nonsymmetric hysteresis loop (Figure 5b, c). Low molar concentration of Fe^{3+} might have caused such variation. The distribution of Fe^{3+} ions in 0.1Fe might be uniform as the hysteresis loop is symmetrical. The magnetization values mainly depend on the charge state of the doped magnetic element. Hence Fe-nHAp attached with drugs (antibiotic or anticancer) may be delivered at the targeted site because of its magnetic property.[3,25,46,47]

The microhardness value of the samples with respect to load was plotted in Figure 6. The hardness value increases with an increase in the incorporation of Fe^{3+} ions. The 0Fe, 0.01Fe, 0.05Fe and 0.1Fe withstood the amount of load in the order of 25, 30, 35, and 40 g and subsequent hardness was found to be 16.5, 25.7, 32.6, and 38 GPa, respectively. The enhancement in hardness values was found to increase by 40% for 0.1Fe compared to nHAP. These results were consistent with the reports available in the literature, that the hardness value (H_v) increases with decrease in the grain size.[48]

Electrical properties of the synthesized nHAp were studied to have an insight into its utility as a matrix for bone growth. Because studies have shown that bone porosity and its interaction with electric field improves fracture healing,[9] we have also investigated the dielectric constant of the samples. The dielectric constant for the 0Fe, 0.01Fe, 0.05Fe, and 0.1Fe shows 150–96, 184–14, 215–15, and 395–19, respectively, at 1 × 10^3 Hz to 1 × 10^6 Hz (Figure 7). A gradual increase in dielectric constant was observed with an increase in Fe^{3+} content. This behavior implies an increase in ionic polarizability of the material and could definitely be attributed to the presence of Fe^{3+} in the nHAp. We anticipate that Fe^{3+}-doped nHAp could support bone growth and promote fracture healing.[8]

The drug release profile of an amoxicillin-incorporated nHAp and Fe^{3+}-doped nHAp pellets was as shown in Figure 8. The 0.01Fe showed prolonged 100% release at 93 h. This may be

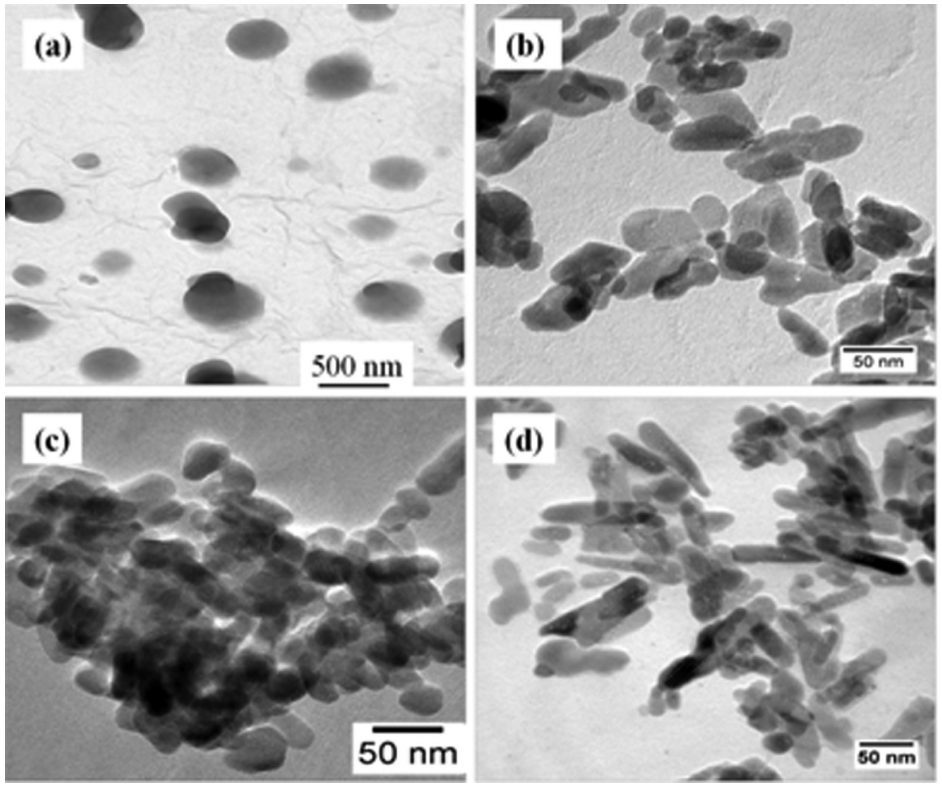

Figure 4. TEM images for Fe^{3+}-doped and undoped HAp samples (a) 0Fe, (b) 0.01Fe, (c) 0.05Fe, and (d) 0.1Fe.

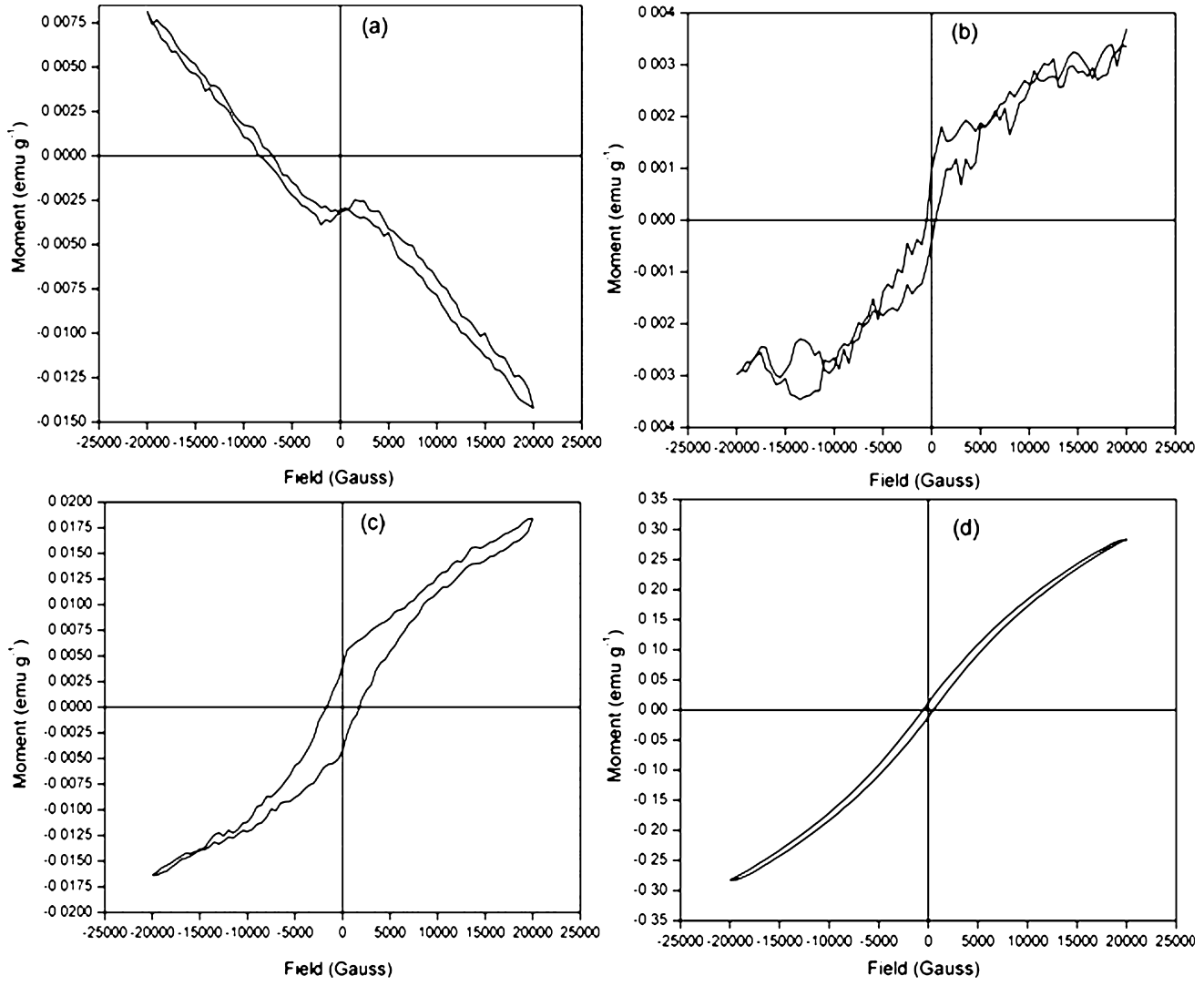

Figure 5. Magnetization curves for undoped and Fe^{3+} doped samples in an applied magnetic field of ± 2 tesla (a) 0Fe, (b) 0.01Fe, (c) 0.05Fe, and (d) 0.1Fe.

Table 5. M_s and M_r of Fe^{3+}-Doped HAp Samples

sample code	magnetization (M_s) (emu g^{-1})	retentivity (M_r) (emu g^{-1})
0.01Fe	0.0036	0.69×10^{-3}
0.05Fe	0.0174	4.09×10^{-3}
0.1Fe	0.2836	11.52×10^{-3}

due to high binding affinity with Fe^{3+} ions to amoxicillin in phosphate buffer saline solution. The release profile for the 0.1Fe is very fast which released 100% of the drug within 45 h, whereas 0Fe- and 0.05Fe-doped nHAp showed 100% release of the drug at 69 and 57 h, respectively.

The drug release profile of an antineoplastic chemotherapy drug 5-fluorouracil incorporated in the undoped and Fe^{3+}-doped nHAp pellets is as shown in Figure 9. Initially, there was a burst release of about 80% for the 0Fe sample at 1.5 h. The samples 0.01Fe, 0.05Fe, and 0.1Fe displayed 50% drug release at 1.5 h. The complete drug release of about 100% for 0Fe sample then occurred at 6 h. The 0.01Fe, 0.05Fe, and 0.1Fe attained 100% release at 18, 12, and 9 h, respectively. Although 0Fe showed rapid release, the 0.01Fe doping leads to a significant decrease in drug release. This implies that Fe^{3+} might be in a covalent bonding with the drug moiety and there by

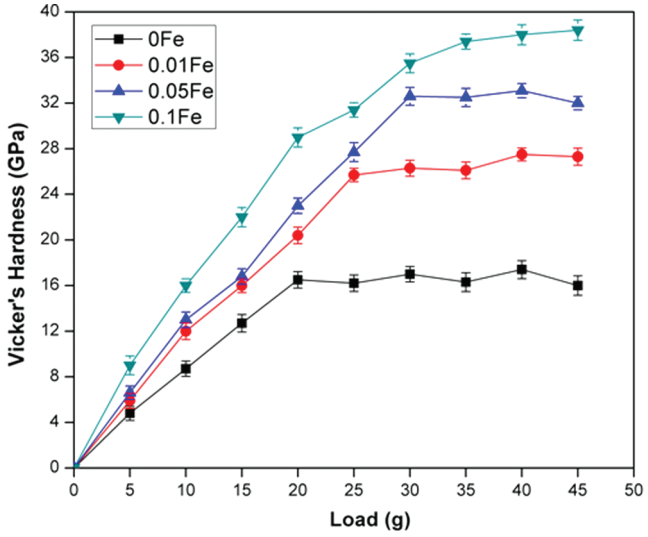

Figure 6. Vickers' hardness (H_v) vs load (g) for the Fe^{3+}-doped and undoped HAp samples (a) 0Fe, (b) 0.01Fe, (c) 0.05Fe, and (d) 0.1Fe.

delaying the release of the latter. But with increase in Fe^{3+} (0.05 and 0.1) the drug release becomes rapid. At 0.05 and 0.1 molar

dx.doi.org/10.1021/am300140q | ACS Appl. Mater. Interfaces 2012, 4, 1200−1210

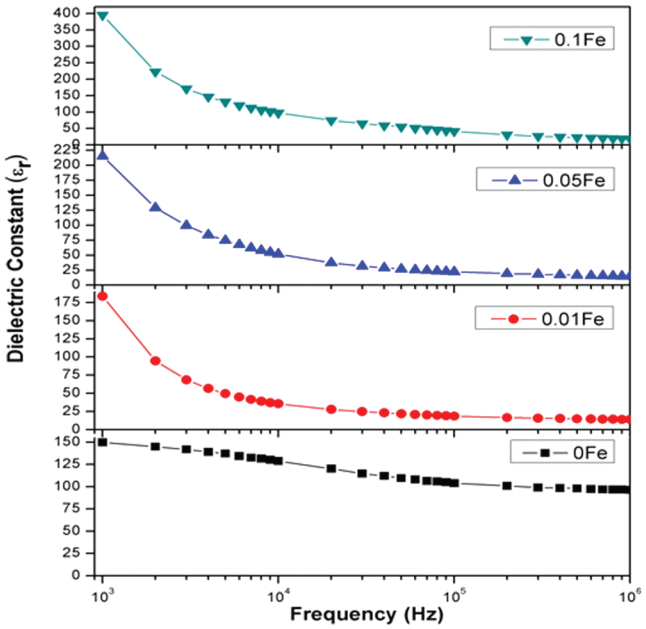

Figure 7. Dielectric constant of Fe^{3+}-doped and undoped HAp samples (a) 0Fe, (b) 0.01Fe, (c) 0.05Fe, and (d) 0.1Fe.

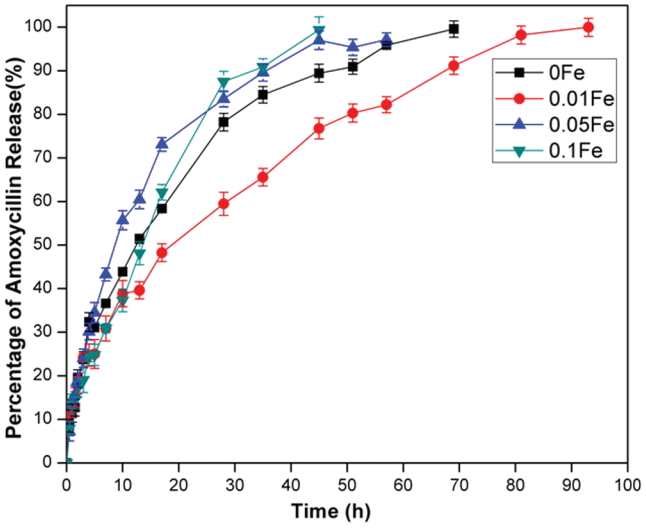

Figure 8. Drug release kinetics for the Fe^{3+}-doped and undoped HAp samples with an antibiotic drug (Amoxicillin) (a) 0Fe, (b) 0.01Fe, (c) 0.05Fe, and (d) 0.1Fe.

doping of Fe^{3+}, drug might have more accessibility bond to Fe^{3+} rather than both Fe^{3+} and nHAp. These results indicate that Fe^{3+} doping delayed 5-fluorouracil release. Hence it is proved that bonding of both nHAp and Fe^{3+} with the drug could be important to ensure delayed release. Thus, Fe^{3+}-doped nHAp could serve as a sustained release depot (a depot injection is an injection, usually subcutaneous or intramuscular, of a pharmacological agent that releases its active compound in a consistent way over a long period of time) for 5-fluorouracil; sustained drug release for cancer chemotherapy could probably circumvent drug resistance an important impediment in cancer therapy. These results correlate with the previous reports, where metal-ion-incorporated nHAp displayed better drug delivery.[11,21,49]

In vitro Biocompatibility Studies. The hemocompatibility of the various concentrations of the Fe^{3+}-doped nHAp

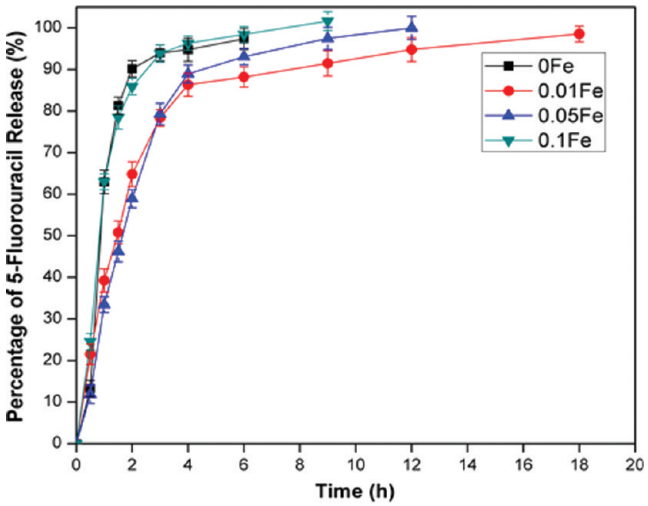

Figure 9. Drug release kinetics for the Fe^{3+}-doped and undoped HAp Samples with an anticancer drug (5-Fluorouracil) (a) 0Fe, (b) 0.01Fe, (c) 0.05Fe, and (d) 0.1Fe.

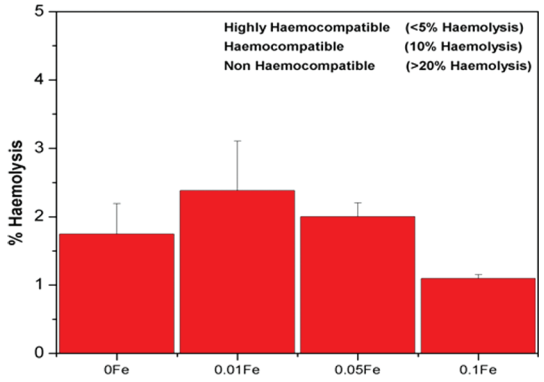

Figure 10. Hemolytic assay for the HAp and Fe-HAp samples (a) 0Fe, (b) 0.01Fe, (c) 0.05Fe, and (d) 0.1Fe.

was tested through hemolytic activity. The results showed that both the undoped and doped samples did not cause hemolysis. The recorded OD values are plotted in the graph (Figure 10). The values obtained were found to be well within the acceptable limits of hemocompatibility for a biomaterial.[50]

The in vitro bioactivity test of the material showed the deposition of the apatite layers on the samples, however there was better apatite layer deposition on the Fe^{3+}-doped nHAp (Figure 11). The increase in apatite layer deposited on the surface of Fe^{3+}-doped nHAp may be due to the drastic reduction in particle size. Nanoscale distinction in the local interface potential is certain to affect the adsorption process of ions and biomolecules in the formation of calcium phosphate (apatite) layers.[51] Apatite layer deposition was further confirmed by the weight gain of the samples before and after soaking in the SBF (Figure 12).[40] The deposition of the apatite layer on the samples surface has also been confirmed by the EDS (Figure 11, insets). From EDS analysis, the Ca/P ratio was calculated to be 1.71, 1.70, 1.89, and 1.77, respectively, for 0Fe, 0.01Fe, 0.05Fe, and 0.1Fe (Figure 11a–d, insets). This confirms Ca rich apatite formation on surface of the SBF soaked samples. In addition, the HAp surface reveal negative surface charges due to the presence of phosphate (PO_4^{3-}) and hydroxyl (OH^-) groups on its surface. These negative ions

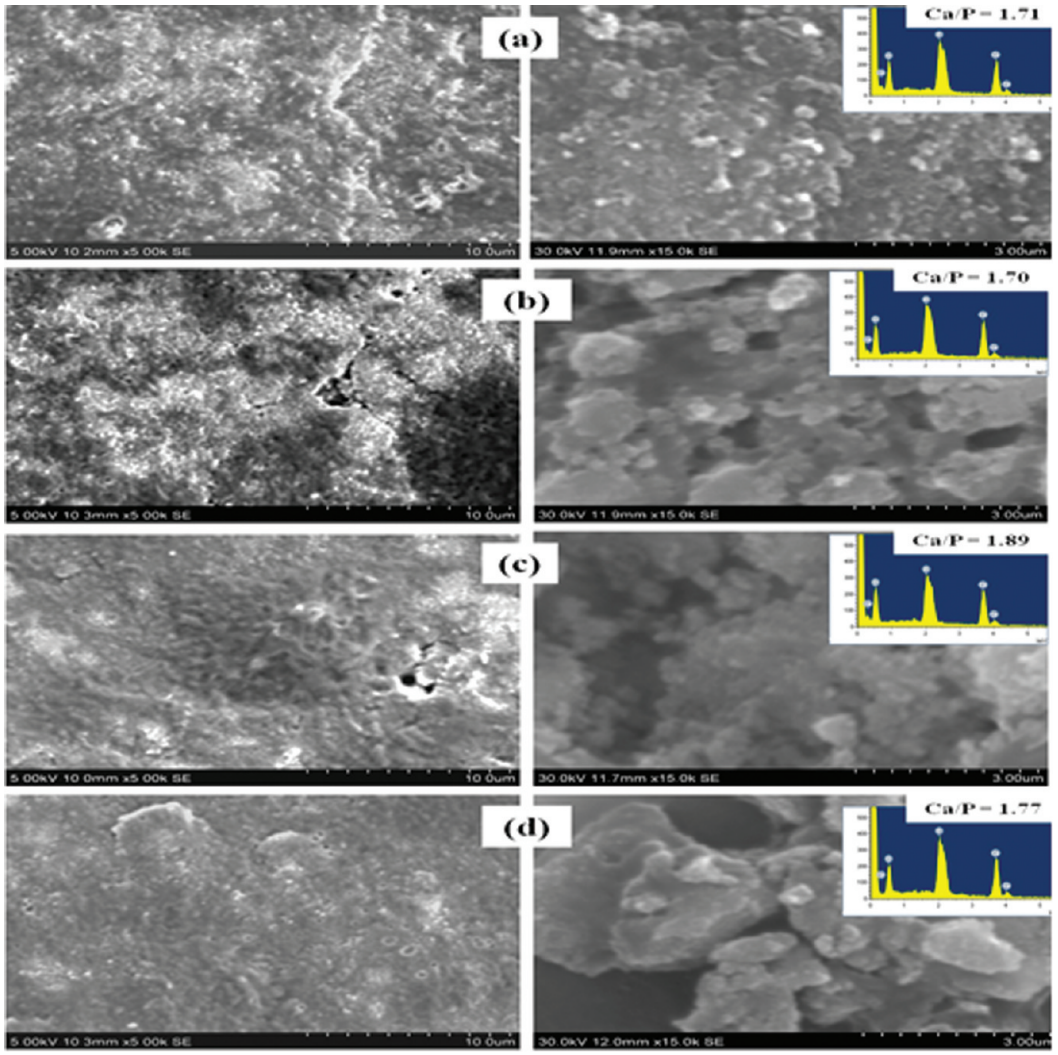

Figure 11. SEM photographs with low and high magnification and EDAX spectra of the SBF soaked samples for 3 weeks (a) 0Fe, (b) 0.01Fe, (c) 0.05Fe, and (d) 0.1Fe (insets, EDAX spectra with Ca/P ratio).

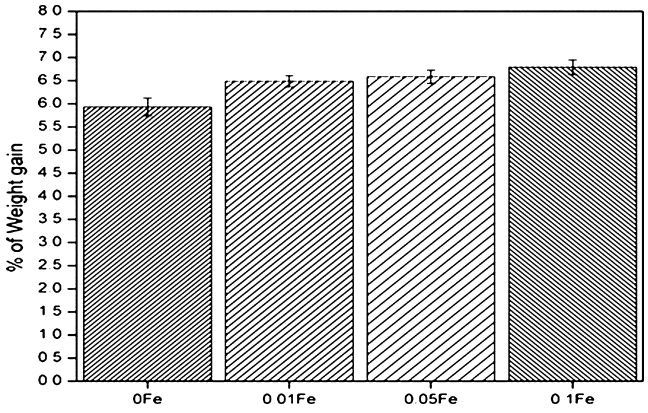

Figure 12. Percentage of weight gain during SBF immersion for 3 weeks (a) 0Fe, (b) 0.01Fe, (c) 0.05Fe, and (d) 0.1Fe.

interact with the positive calcium ions in the SBF to form the Ca-rich ACP (amorphous calcium phosphate), which gain positive surface charge. The Ca-rich ACP interacts with the negative phosphate ions in the SBF to form the Ca-poor ACP, which stabilizes by being crystallized into bonelike apatite in the SBF.[52]

The antibacterial efficacy of the amoxicillin impregnated undoped and doped nHAp against *E. coli*, *S. epidermidis*, and *S. aureus* was as shown in Figure 13. The zones of inhibition observed for the various pellets used were measured (Table 6). The efficacy against *E. coli* showed the highest zone of inhibition when compared to the other species tested. The 0.01Fe drug loaded samples show highest zone of inhibition against the microorganisms such as *E. coli*, *S. epidermidis*, and *S. aureus*. Therefore, the drug release profile with an antibiotic shows similar results in the antibacterial efficacy against microorganisms. 0.01Fe exhibits controlled and extended drug release profile and highest zone of inhibition due to high binding affinity of nHAp with the drug. Thus, 0.01Fe nHAp impregnated with antibiotic showed efficacy against the common pathogens *E. coli*, *S. epidermidis*, and *S. aureus* implicated for the long-term treatment in osteomyelitis.

The proliferation of MG-63 cells in the presence of undoped and doped HAp samples examined was as illustrated in Figure 14. It is evident from the results that the undoped samples show better cell proliferation with more than 90% of viable cells, whereas the doped 0.01Fe, 0.05Fe and 0.1Fe

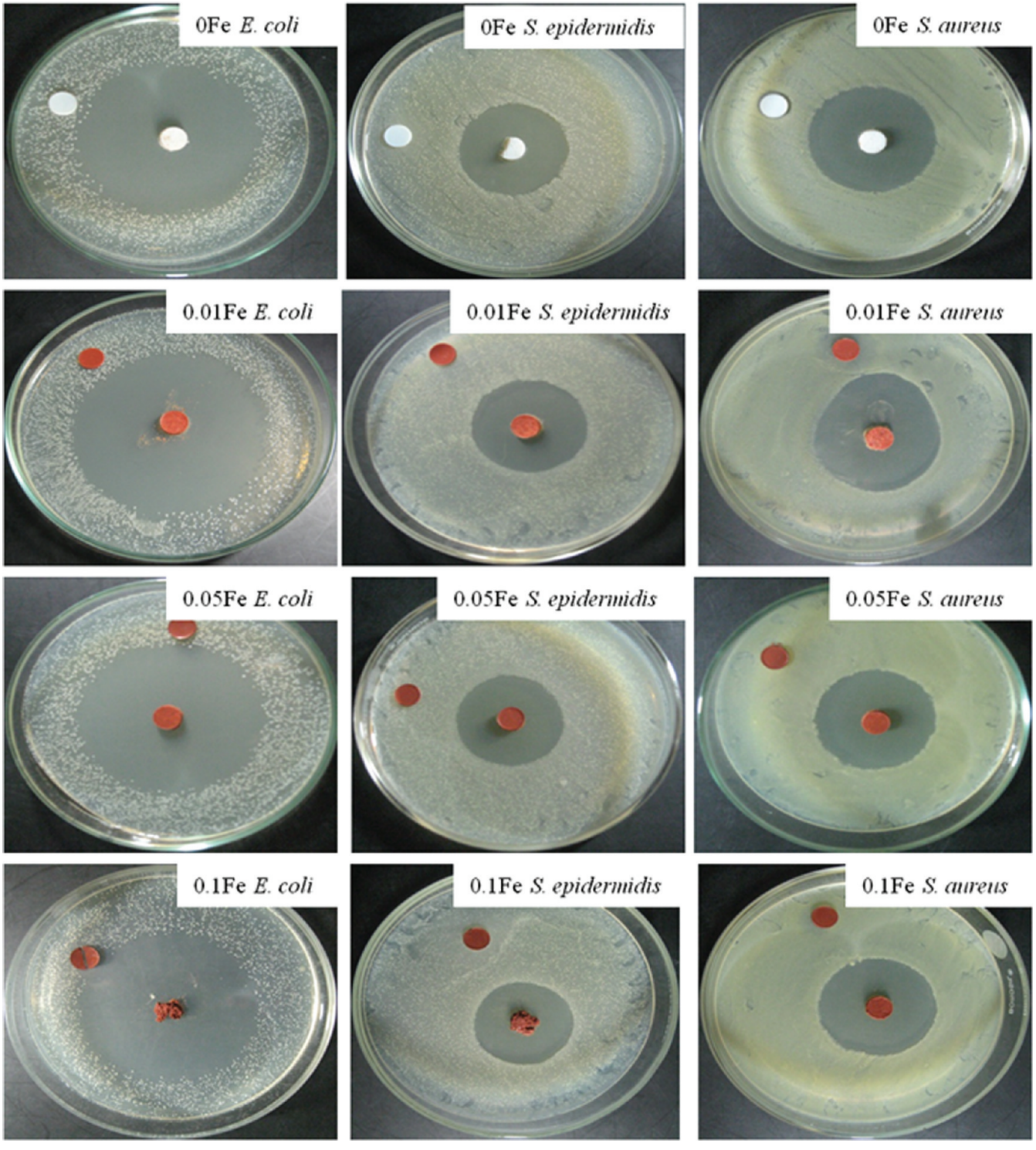

Figure 13. Agar diffusion test for the Fe^{3+} doped and undoped HAp samples with *E. coli*, *S. epidermidis*, and *S. aureus* (a) 0Fe, (b) 0.01Fe, (c) 0.05Fe, and (d) 0.1Fe.

Table 6. Zone of Inhibition of the Antibacterial Efficacy Against *E. coli*, *S. epidermidis*, and *S. aureus*

	diameter of inhibition zone (±0.5 mm)			
bacterial strain	0Fe	0.01Fe	0.05Fe	0.1Fe
E. coli	5.7	5.9	5.6	5.5
S. epidermidis	3.4	3.5	3.3	3.2
S. aureus	3.8	4.0	3.7	3.8

show a significant increase in the cell proliferation on day 3 compared to day 1 with the percentage of cell viability ranging between 65% and 80% of viable cells. The results indicate that the doped and undoped samples support the proliferation of MG-63 cells. The studies on hemocompatibility, antimicrobial efficacy, and MTT assay reveal that Fe-nHAp is noncytotoxic and biocompatible. Li et al. reported the non-cytotoxic nature of the Fe-nHAp ceramics.[3]

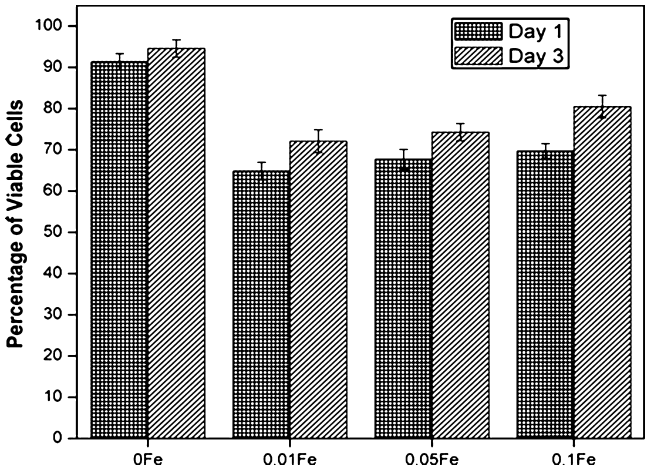

Figure 14. Percentage of viable cells with MG63 cells treated on HAp and Fe-HAp samples for day 1 and day 3 (a) 0Fe, (b) 0.01Fe, (c) 0.05Fe, and (d) 0.1Fe.

4. CONCLUSIONS

In summary, undoped and Fe^{3+}-doped nHAp were synthesized by a combination of hydrothermal and microwave techniques. The crystallite size and the crystallinity decreased with an increase in Fe^{3+} content. The functional groups of nHAp were characterized by FT-IR. The spherical nHAp (200 ± 5 nm) is modified on Fe^{3+} doping, into rodlike structures, with a considerable reduction in average size (75 ± 5 nm). The maximum hardness of 0.1Fe showed 38 GPa with a particle size of 75 ± 5 nm, whereas 0Fe showed 16.5 GPa with a particle size of 200 ± 5 nm. These results suggest that the Fe^{3+} doping decreases the particle size along with a significant increase in hardness. The Fe^{3+}-doped samples showed hysteresis loop indicating superparamagnetic behavior, whereas nHAp was diamagnetic. The increasing trend in dielectric constant values on Fe^{3+}-doped nHAp shows remarkable polarizability of this material. The hemolytic assay proved that Fe^{3+}-doped nHAp is a blood compatible biomaterial. The drug release studies performed with the antibiotic (amoxicillin) and anticancer (5-Fluorouracil) drugs showed that Fe^{3+} doping at a low concentration of about 8 ppm leads to highly prolonged drug release. In addition, the Fe^{3+} doping led to an increase in the bioactivity when tested in SBF. The growth of the apatite layer on the samples surface has been confirmed by EDS analysis of the deposited layer. The antibacterial efficacy as determined against *E. coli*, *S. aureus*, and *S. epidermidis* by the agar diffusion test showed that this biomaterial will be useful in treatment of bone and joint infections. Hence, the proliferative potential for undoped and doped samples showed noncytotoxic by MTT assay in MG63 osteosarcoma cells. Further in vivo studies will be performed in mice model. Sustained drug release systems developed in the present study would be a useful approach to treat malignant tumors, because it overcomes the impediments of treatment-induced drug resistance and nonspecific systemic toxicity.

AUTHOR INFORMATION

Corresponding Author

*Phone: +91 44 22208335. Fax: +91 44 22352774. E-mail: kalkura@yahoo.com or kalkurasn@annauniv.edu (S.N.K.); Phone: +91 44 2476 5512, extension 237. Fax: +91 44 2476 7008. gvenkat16@gmail.com (G.V.).

Notes

The authors declare no competing financial interest.

ACKNOWLEDGMENTS

S.C.V. gratefully acknowledges AICTE, New Delhi, India, for the financial assistance as a National Doctoral Fellowship (File 1-10/RID/NDF-PG/(45)2008-09) and DBT, New Delhi, through Research Project BT/PR11799/MED/32/103/2009. The authors thank Dr. M. Palanichamy, Department of Chemistry, Anna University, Chennai, for valuable discussions and Dr. K. Sivakumar, Department of Physics, Anna University, for help in characterizing the samples.

REFERENCES

(1) Narbat, M. K.; Orang, F.; Hashtjin, M. S.; Goudarzi, A. *Iran. Biomed. J.* **2006**, *10*, 215−223.
(2) Komlev, V. S.; Barinov, S. M.; Koplik, E. V. *Biomaterials* **2002**, *23*, 3449−3454.
(3) Li, Y.; Nam, C. T.; Ooi, C. P. *J. Phys. Conf. Ser.* **2007**, *187*, 012024.
(4) Dash, A. K.; Cudworth, G. C. II. *J. Pharmacol. Toxicol. Methods* **1998**, *40*, 1−12.
(5) Xu, Q.; Czernuszka, J. T. *J. Controlled Release* **2008**, *127*, 146−153.
(6) Pham, H. H.; Luo, P.; Genin, F.; Dash, A. K. *AAPS Pharm. Sci. Technol.* **2002**, 3.
(7) Baro, M.; Sánchez, E.; Delgado, A.; Perera, A.; Évora, C. *J. Controlled Release* **2002**, *83*, 353−364.
(8) Quilitz, M.; Steingröver, K.; Veith, M. *J. Mater. Sci.−Mater. Med.* **2010**, *21*, 399−405.
(9) Hoepfner, T. P.; Case, E. D. *J. Biomed. Mater. Res., A* **2002**, *60*, 643−650.
(10) Gittings, J. P.; Bowen, C. R.; Turner, I. G.; Dent, A. C. E.; Baxter, F. R.; Chaudhuri, J. B. *Acta Biomater.* **2009**, *5*, 743−754.
(11) Joshy, M. I. A.; Elayaraja, K.; Suganthi, R. V.; Veerla, S. C.; Kalkura, S. N. *Curr. Appl. Phys.* **2011**, *11*, 1100−1106.
(12) Filho, F. P.; Nogueira, R. E. F. Q.; Graça, M. P. F; Valente, M. A.; Sombra, A. S. B.; Silva, C. C. *Physica B* **2008**, *403*, 3826−3829.
(13) Bose, S.; Dasgupta, S.; Tarafder., S.; Bandyopadyay, A. *Acta Biomater.* **2010**, *6*, 3782−3790.
(14) Jadalannagari, S.; More, S.; Kowshik, M.; Ramanan, S. R. *Mater. Sci. Eng., C.* **2011**, *31*, 1534−1538.
(15) Zhou, H.; Lee, J. *Acta Biomater.* **2011**, *7*, 2769−2781.
(16) Ribeiro, N.; Sousa, S. R.; Monteiro, F. J. *J. Colloid Interface Sci.* **2010**, *351*, 398−406.
(17) Peng, F.; Yu, X.; Wei, M. *Acta Biomater.* **2011**, *7*, 2585−2592.
(18) Huang, J.; Best, S. M.; Bonfield, W.; Buckland, T. *Acta Biomater.* **2010**, *6*, 241−249.
(19) Webster, T. J.; Massa-Schluter, E. A.; Smith, J. L.; Slamovich, E. B. *Biomaterials* **2004**, *25*, 2111−2121.
(20) Wakamura, M.; Kandori, K.; Ishikawa, T. *Colloids Surf., A* **2000**, *164*, 297−305.
(21) Suganthi, R. V.; Elayaraja, K.; Joshy, M. I. A.; Veerla, S. C.; Girija, E. K.; Kalkura, S. N. *Mater. Sci. Eng., C.* **2011**, *31*, 593−599.
(22) Stojanovic, Z.; Veselinovic, L .; Markovic, S.; Ignjatovic, N.; Uskokovic, D. *Mater. Manuf. Process.* **2009**, *24*, 1096−1103.
(23) Ajeesh, M.; Francis, B. F.; Annie, J.; Varma, P. R. H. *J. Mater. Sci.−Mater. Med.* **2010**, *21*, 1427−1434.
(24) Morrissey, R.; Rodrigue-Lorenzo, L. M.; Gross, K. A. *J. Mater. Sci.−Mater. Med.* **2005**, *16*, 387−392.
(25) Wu, H. C.; Wang, T. W.; Sun, J. S.; Wang, W. H.; Lin, F. H. *Nanotechnology* **2007**, *18*, 165601.
(26) Lieu, P. T.; Heiskala, M.; Peterson, P. A.; Yang, Y. *Mol. Aspects Med.* **2001**, *22*, 1−87.
(27) Saeri, M. R.; Afshar, A.; Ghorbani, M.; Ehsani, N.; Sorrell, C. C. *Mater. Lett.* **2003**, *57*, 4064−4069.

(28) Anee, T. K.; Palanichamy, M.; Ashok, M.; Sundaram, N. M.; Narayana Kalkura, S. *Mater. Lett.* **2004**, *58*, 478−482.
(29) Mardziah, C. M.; Sopyan, I.; Ramesh, S. *Trends Biomater. Artif. Organs* **2009**, *23*, 105−113.
(30) Li, M'O.; Xiao, X.; Liu, R.; Chen, C.; Huang, L. *J. Mater. Sci.−Mater. Med.* **2008**, *19*, 797−803.
(31) Pon-On, W.; Meejo, S. *Int. J. Nanosci.* **2007**, *6*, 9−16.
(32) Ashok, M.; Narayana Kalkura, S.; Sundaram, N. M.; Arivuoli, D. *J. Mater. Sci.−Mater. Med.* **2007**, *18*, 895−898.
(33) Lak, A.; Mazloumi, M.; Mohajerani, M. S.; Zanganeh, S.; Shayegh, M. R.; Kajbafvala, A.; Arami, H.; Sadrnezhaad, S. K. *J. Am. Ceram. Soc.* **2008**, *91*, 3580−3584.
(34) Vani, R.; Raja, S. B.; Sridevi, T. S.; Savithri, K.; Devaraj, S. N.; Girija, E. K.; Thamizhavel, A.; Kalkura, S. N. *Nanotechnology* **2011**, *22*, 285701.
(35) Han, J.; Song, H.; Saito, F.; Lee, B. *Mater. Chem. Phys.* **2006**, *99*, 235−239.
(36) Singhal, J. P.; Ray, A R. *Biomaterials* **2002**, *23*, 1139−1145.
(37) Komath, M.; Varma, H. K. *Bull. Mater. Sci.* **2003**, *26*, 415−422.
(38) Chowdhury, S. K. R.; Mishra, A.; Pradhan, B.; Saha, D. *Wear* **2004**, *256*, 1026−1036.
(39) Kokubo, T. *J. Non-Cryst. Solids* **1990**, *120*, 138.
(40) Rekola, J.; Lassila, L. V. J; Hirvonen, J.; Lahdenperä, M.; Grenman, R.; Aho, A. J.; Vallittu, P. K. *J. Mater. Sci.−Mater. Med.* **2010**, *21*, 2345−2354.
(41) Rusu, V. M.; Ng, C.; Wilke, M.; Tiersch, B.; Fratzl, P.; Peter, M. G. *Biomaterials* **2005**, *26*, 5414−5426.
(42) Desgreniers, S.; Lagarec, K. *J. Appl. Crystallogr.* **1994**, *27*, 432−434.
(43) Rehman, I.; Bonfield, W. *J. Mater. Sci.−Mater. Med.* **1997**, *8*, 1−4.
(44) Suganthi, R. V.; Girija, E. K.; Kalkura, S. N.; Varma, H. K.; Rajaram, A. *J. Mater. Sci.−Mater. Med.* **2009**, *20*, S131−S136.
(45) Sanvicens, N.; Marco, M. P. *Trends Biotechnol.* **2008**, *26*, 425−433.
(46) Yang, J.; Lee, C. −H.; Ko, H. −J.; Suh, J. −S.; Yoon, H. −G.; Lee, K.; Huh, Y. −M.; Haam, S. *Angew. Chem., Int. Ed.* **2007**, *46*, 8836−8839.
(47) Douziech-Eyrolles, L.; Marchais, H.; Hervé, K.; Munnier, E.; Soucé, M.; Linassier, C.; Dubois, P.; Chourpa, I. *Int. J. Nanomed.* **2007**, *2* (4), 541.
(48) Wang, J.; Shaw, L. L. *Biomaterials* **2009**, *30*, 6565−6572.
(49) Dasgupta, S.; Banerjee, S. S.; Bandyopadhyay, A.; Bose, S. *Langmuir* **2010**, *26*, 4958−4964.
(50) Pal, K.; Bag, S.; Pal, S. *J. Porous Mater.* **2008**, *15*, 53−59.
(51) Vandiver, J.; Dean, D.; Patel, N.; Bonfield, W.; Ortiz, C. *Biomaterials* **2005**, *26*, 271−283.
(52) Suganthi, R. V.; Parthiban, S. P.; Elayaraja, K.; Girija, E. K.; Kulariya, P.; Katharria, Y. S.; Singh, F.; Asokan, K.; Kanjilal, D.; Kalkura, S. N. *J. Mater. Sci.−Mater. Med.* **2009**, *20*, S271−S275.